Fatigue crack propagation for a through thickness crack: a crack propagation law considering cyclic plasticity near the crack tip

Toyosada, Masahiro
Department of Marine Systems Engineering, Kyushu University

Gotoh, Koji
Department of Marine Systems Engineering, Kyushu University

Niwa, Toshio
National Maritime Research Institute Japan, Materials Reliability Group

出版情報：International Journal of Fatigue. 26 (9), pp.983-992, 2004-09. Elsevier
バージョン：
権利関係：

Fatigue Crack Propagation for a Through Tickness Crack: A crack propagation law considering cyclic plasticity near the crack tip

Masahiro Toyosada [a,*] , Koji Gotoh [a] and Toshio Niwa [b]

[a] *Kyushu University, Department of Marine Systems Engineering, 6-10-1, Hakozaki, Higashi-ku, Fukuoka, 812-8581, Japan*

[b] *National Maritime Research Institute Japan, Materials Reliability Group, 6-38-1, Shinkawa, Mitaka, Tokyo, 181-0004, Japan*

Abstract

A new parameter, which can quantitatively describe fatigue crack propagation, is proposed in this paper. This parameter reflects the cyclic plasticity behaviour near the crack tip, and the resulting built up of layers with the residual plastic deformations on the fatigue crack surfaces. A fatigue crack closure model suitable for an arbitrary applied stress distribution with an arbitrary residual stress distribution based on appropriately modified Dugdale's concept of crack tip plasticity is developed. An RPG (Re-tensile Plastic zone Generated) load, at which the tensile plastic zone starts to develop ahead of a crack tip, is defined. The effective stress intensity factor range is redefined by replacing the crack opening load with the RPG load. This redefined effective stress intensity factor is termed ΔK_{RPG}. When ΔK_{RPG} substitutes for ΔK or the crack opening load based on ΔK_{eff} the "knee"

in the threshold region of the crack growth data is not seen any longer. As a result, it is confirmed that a stopping phenomenon of a fatigue crack propagation can be quantitatively and appropriately described without the threshold value such as $(\Delta K_{eff})_{th}$. It is also confirmed that the proposed crack closure model can provide quantitative estimates of the fatigue life under various loading conditions and in pre-existing residual stress field.

Key words: Fatigue crack closure model, Cyclic plasticity, RPG (Re-tensile Plastic zone Generated) load, ΔK_{RPG}, Threshold of stress intensity factor range

1 Fatigue Crack Propagation Law Based on Crack Closure

Paris and Erdogan [1] proposed a fatigue crack propagation equation, the so called "Paris' law". At that time most researchers were believing that a fatigue crack opens during cyclic loading, because according to the Dugdale model [2] calculation results of the crack opening displacement at the minimum load (P_{min}) following the maximum load show that the crack opens. Then Elber [3] pointed out that fatigue cracks remained closed during a part of load cycles because the fatigue crack propagated in the residual tensile plastic deformed zone ahead of the crack tip. He proposed an effective stress intensity factor range in the replacement of the stress intensity factor range in Paris' law to be used as the fatigue crack propagation parameter.

Figure 1 shows a schematic change of the plastic deformation and the work-

* Tel.:+81-92-642-3713
Email address: toyosada@nams.kyushu-u.ac.jp (Masahiro Toyosada).
URL: http://www.nams.kyushu-u.ac.jp/common/production/index_e.html (Masahiro Toyosada).

ing stress distribution along the crack line in one loading cycle during the fatigue crack propagation. It becomes clear from the detailed consideration of the crack opening/closing phenomena and the generation and growth of the plastic zone throughout one loading cycle loading that the plastic work is not proceeded in the loading range from crack opening load (P_{op}) to Re-tensile Plastic zone's Generated load (RPG load, P_{RPG}). There is no stress singularity due to the crack at P_{op}, because the compressive (contact) stresses in the crack closure region release just before this moment, as shown in Fig.1(b). Stress at the crack tip increases very rapidly just after the loading because of very large stress concentration. However just when at the P_{RPG} level stress at the crack tip reaches the value of the material yield stress, the stress distribution ahead of the crack tip has still an indentation as shown in Fig.1(c). More applied loading is necessary in order to develop the tensile plastic zone ahead of a crack tip. For cyclic loading, the gradient of the elastic stress distribution near the crack tip under the increasing load is steeper than for monotonic loading, as shown in Fig.2, because the notch tip acuity of the fatigue crack is larger than that of a crack under monotonic loading. The blunting of a crack tip is caused in the case of monotonic loading. Therefore, the plastic zone development under cyclic loading is slower than under monotonic loading.

A subraction electronic circuit in order to measure the P_{op} and the P_{RPG} load levels is developed by authors. The identification method of the P_{RPG} load is explained in the reference [4].

The measurment results indicate that P_{RPG} is higher than P_{op} except when a fatigue crack propagates in a compressive residual stress field (When a fatigue crack propagates in large compressive residual stress field, P_{RPG} is usually equal to P_{op} [5]). Although a changing tendency of P_{RPG} is almost same as

that of P_{op} under stationary cyclic loading, these loads can show a different behaviour under some conditions [6].

P_{op} approaches P_{min} and P_{RPG} approaches P_{max} as the crack growth stops under the stepwise decreasing amplitude loading while P_{max} keeps the constant value, because the crack tends to remain open and shows no cyclic plasticity at the final stage [6]. Therefore, the threshold phenomenon does not appear in the relation between $\Delta K_{RPG}(= (P_{max} - P_{RPG})\sqrt{\pi a} f$, where f: magnification factor, a: crack length) and the fatigue crack propagation rate, as shown in Fig.3, but it does appear in the relation between $\Delta K_{eff}(= (P_{max} - P_{op})\sqrt{\pi a} f)$ and the fatigue crack propagation rate, as shown in Fig.4. Mild steel is used for the specimens in Figs.3 and 4. The equation of fatigue crack propagation can be described by

$$da/dN = C(\Delta K_{RPG})^m \tag{1}$$

where C, m: material constants.

Figure 5 shows a schematic change of the crack deformations and the working stress distribution when the crack stops growing during a loading cycle. Since neither a tensile plastic zone at the maximum load nor a compressive plastic zone at the minimum load (or both) appear in the loading cycle in that case, no plastic work is consumed during this loading cycle. It is considered that loading range from P_{min} to P_{RPG} corresponds to ΔK_{th} and that from P_{op} to P_{RPG} corresponds to $(\Delta K_{eff})_{th}$ at a limit condition when a crack propagation stops. These changes of crack deformation and applied stress distribution show entirely different behaviour as a result of crack propagation in the loading range from P_{min} to P_{RPG}. This loading range does not relate to crack propagation force, as a result of the comparison Fig.5 with Fig.1. The distribution of resid-

ual tensile deformations around the crack tip under variable amplitude loading is quite different from that under constant amplitude loading and the closure regions are different in each case. Then ΔK_{th} or $(\Delta K_{eff})_{th}$, which is obtained from the constant amplitude test or the gradually decreasing amplitude test, has no relation with the stopping condition under variable amplitude loading.

2 Crack opening and closing model for a through thickness fatigue crack

The condition of the displacement continuity ahead of the physical crack tip is not satisfied in the original Dugdale model. To eliminate this deficiency we postulate that the chink corresponding to the virtual COD in the plastic zone should be plugged up by a small segment of elastic-plastic material shown by the shaded zone in Fig.6(a). The physical meaning of the virtural COD is investigated in the reference [7].

After loading the segment with uniform elastic stresses of the yield stress magnitude under an appropriate triaxial constraint condition, it deforms elastically to accurately fit the fictitious COD in the plastic zone of Dugdale model, as indicated by the solid line in Fig.6(b). Inserting the segments enables to satisfy the displacement continuity and improves the model performance compared to the original Dugdale concept.

The advantage of the proposed approach can be proved by considering Newman's crack closure model [8] for which the segment material is assumed to be rigid-plastic. In his model, the crack opening load is given by

$$K(P_{op} - P_{min}) - K(\text{contact stress}) = 0. \tag{2}$$

The first term in the right side shows the change of the stress intensity from the minimum load to the crack opening load. The second term represents the stress intensity caused by the contact stress distribution worked on the crack closure region at the minimu load. Although equation (2) appears correctly at the first sight, P_{op} by this equation gives lower value than actual one, because release of the contact stress acts to proceed the compressive plastic zone and shrinking COD. More load increment is necessary to release the contact stress completely. Then he assumed a very high plastic constraint factor (even larger than 3) for getting large P_{op}, because his model gives smaller P_{op} than measured one [9]. Moreover, in posterior works [10] Newman changes a value of plastic constraint factor in response to fatigue crack propagation rates in order to coincide the computed results with experimental data.

If the current tensile plastic zone extends beyond the previous plastic zone, the original Dugdale model should be satisfied. A layer of the residual tensile deformations generated by the previous loading is on the fatigue crack surface. The thickness of the layer L_j is assumed to equal length of the segment after removing the applied stress, because the perfect elastic-plastic material of the layer is assumed.

$$L_j = V_j/(1 + \lambda\sigma_Y/E'), \tag{3}$$

where

$$E' = \begin{cases} E & \text{(plane stress condition)} \\ E/(1-\nu^2) & \text{(plane strain condition)}, \end{cases}$$

V_j: fictitious COD at x_j in a plastic zone which is beyond the previous plastic zone at maximum load,

L_j: thickness of the plasticity elongated layer at x_j,

σ_Y: material yield strength,

λ: plastic constraint factor,

E: Young's modulus,

ν: Poisson's ratio.

If the present plastic zone is embedded in the previous plastic zone, the superposition principle shown in Fig.7 is satisfied based on the Dugdale model and the following relations are introduced [11].

$$V_j = P\sum_{i=1}^{n} s_i F(x_j, x_i, a^*) - \sum_{i=1}^{n} \sigma_i F(x_j, x_i, a^*) + \sum_{i=1}^{n} \sigma_i^R F(x_j, x_i, a^*), \qquad (4)$$

where

V_j: COD at x_j when external load is P,

P : magnitude of the external load,

s_i: applied stress at x_i per unit external load,

a^*: length of the fictitious crack (tip of the tensile plastic zone),

$F(x_j, x_i, a^*)$: COD at x_j when a uniform unit stress acts betweenB_i and B_{i+1} on the crack surfaces,

$x_i = (B_i + B_{i+1})/2$,

σ_i^R: pre-existing residual stress at x_i,

σ_i: working stress at x_i along the crack line.

If an element remains elastic, the following relation should be satisfied in the fictitious crack region and the crack closure region.

$$V_j = (1 + \sigma_j/E')L_j. \tag{5}$$

By substituting Eq.(4) into Eq.(5), σ_j can be obtained by solving the resulting linear system of equations through an iterative method with the following constraints added:

For the region ahead of the crack tip,

$$\text{if } \sigma_j < -\lambda\sigma_Y, \quad \text{then } \sigma_j = -\lambda\sigma_Y$$

and

$$\text{if } \sigma_j > \lambda\sigma_Y, \qquad \text{then } \sigma_j = \lambda\sigma_Y.$$

For the plastic wake zone (the real crack surface),

$$\text{if } \sigma_j > 0, \qquad \text{then } \sigma_j = 0$$

and

$$\text{if } \sigma_j < -\lambda\sigma_Y, \quad \text{then } \sigma_j = -\lambda\sigma_Y.$$

From the solution of σ_j , COD is obtained by Eq.(4) at P_{min} or P_{max} if the tensile plastic zone is inside the previous tensile plastic zone.

Schematically the distributions of COD and stress at the minimum load are shown in Fig.8. $\hat{V}_j$ in Fig.8 indicates the COD at the minimum load with crack length of c, i.e. just before the fatigue crack initiation. This situation is named e.c. Case A in the figure. $\tilde{V}_j$ in Fig.8 indicates the COD at the minimum load with crack length of $c + \Delta c$, i.e. after releasing the contact stresses over crack surfaces in the crack wake zone and the fatigue crack propagation. This situation is named Case B in the figure. σ_j corresponds to the working stress at the minimum load.

If the contact stresses do not occur in the crack wake at P_{min}, the compressive plastic zone grows and then the COD decreases as shown in case C in Fig.8. The distributions of stresses and COD ($\tilde{V}_j$) after a crack extension at P_{min}

associated with an entire release of the contact stress in the crack closure region are also shown by dotted lines as case B in Fig.8.

Fatigue crack propagation during a fatigue cycle can occur on either unloading or loading. If a fatigue crack propagates on unloading, compressive stresses in the region of the crack extension will release just after the extension. The thickness of the plastically elongated layer in the crack extension region at the moment of the crack extension might be less than $\hat{V}_j$ and greater than $\tilde{V}_j$. If the crack propagates on loading, the tensile stresses in the region of the crack extension will release just after crack extension.

The release rate of the contact stresses should change in accordance with the timing of the crack extension during a loading cycle [12]. The same holds true for the rate of the plastic shrinkage (δ_j, see Fig.8). It is assumed that the shrinkage rate depends on the cumulative plastic strain in the crack extension region. Hence, lengths of the bar elements on the crack surface newly created after the crack extension are given by Eq.(6). Because the development of the shrinkage (or expansion) of the bar elements during the loading cycle cannot be precisely described, a cofficient (κ) is defined by Eq.(7) is introduced. The meaning of γ_e and γ_{pi} in this equation is explained in Fig.9.

$$L_j = \hat{V}_j/(1 - \lambda\sigma_Y/E') - \kappa\delta_j. \tag{6}$$

$$\kappa = \begin{cases} \alpha\Delta\varepsilon_p(\gamma_e/\gamma_{pi}) \text{ for } \alpha\Delta\varepsilon_{\mathrm{p}} < 1 \\ 1 \qquad\qquad\quad \text{for } \alpha\Delta\varepsilon_{\mathrm{p}} \geq 1, \end{cases} \tag{7}$$

$$\Delta\varepsilon_p = \left\{(1 - \lambda\sigma_Y/E')(V_j)_{max} - (1 + \lambda\sigma_Y/E')(\hat{V}_j)_{min}\right\}/(V_j)_{max}, \tag{8}$$

where

α: plastic shrinkage coefficient

(material constant: positive value means shrinkage

and negative value means expansion),

$\Delta\varepsilon_p$: plastic strain range.

The RPG load is obtained when the stress in the bar element adjacent to a crack tip reaches the yield stress during the loading reversal. The selection of the value of α in Eq.(7) for mild steel will be addressed later on.

The plastic constraint factor (λ) for mild steel was identified 1.04 on the basis of the experimental results reported in the literature [13]. The plate thickness of the specimens mentioned above is 6mm. The elastic-plastic finite element analysis with the elastic perfectly plastic material under plane stress condition gave the COD profile very close to the results by the Dugdale model in plane stress condition with $\lambda = 1.03$ during the loading [14]. It might be considered that the difference of 0.01 in the constraint factor according to the FE analyses and the experiments comes from strain hardening for mild steel.

3 Numerical Simulation of Fatigue Crack under Various Loading Conditions

Figure 10 shows the effect of stress ratio on fatigue crack propagation. Figure 10(a) shows a center notched specimen used for the experiments. Fatigue crack propagation tests, at stress ratios of 0.05, 0.3 and 0.5, were performed. During

the tests, the RPG loads were measured using a system developed by the authors [4]. The open circles in Figs.10(c),(d) and (e) show the measured RPG load for each test.

The RPG load was calculated using the above proposed fatigue crack closure simulation model with $\lambda = 1.04$. The plastic shrinkage coefficient (α) was selected by trial and error to match the values of the RPG load computed for the stress ratio of 0.05 test with the observed ones. The simulation results obtained for several values of α are shown in Fig.10(c). The best agreement between both type results was obtained for α equal to 0.18 and all the remaining simulations were performed for that value α and λ of 1.04.

At the same time, the influence of the size of the bar element adjacent of the crack tip is investigated by comparing RPG load between measured and calculated under the loading condition of Fig.10(c). This discretization adjacent of the crack tip is identified 0.001mm after the above comparison and fixed throughout all the numerical crack closure simulations for the convenience. The physical meaning of the discretizaion size corresponds to the average moving distance of the dislocation in the first grains at the crack front under one cyclic loading process on the basis of the dislocation theory. This length can be estimated the half of the average grain diameter of the material. Although fixed value (0.001mm) is a little bit smaller than the average of the steels, but the difference is not so serious.

The corresponding simulation results for the stress ratios of 0.3 and 0.5, are shown as the solid curves in Figs. 10(d) and (e) respectively. The calculated fatigue crack growth curves obtained based on the calculated RPG loads and material constants of fatigue crack propagation rate (C and m) according

to Fig.3 are compared with the experimental data in Fig.10(b). The initial crack length of 2mm was set for all the calculations. It is confirmed in Fig.10 that the effect of stress ratio on fatigue crack propagation can be evaluated quantitatively by applying the proposed model.

Fig.11 shows the change of the RPG load and the fatigue crack growth curves in the case of a block loading with the step-down in the maximum load. Specimens used in these experiments were the same as that shown in Fig.10(a). All results indicate that RPG load increases just after the step-down in the maximum load. This is so because the crack closure region at the minimum load extends due to decrement of the thickness of the residual tensile layer in the crack increment region and decreasment of COD just after the maximum load. Consequently,the crack closure region extends over the crack surfaces at the minimum load and the RPG load increases. The delayed reterdation effect increases with increasing the reduction ratio of the the maximu load (ξ). ξ is defined by the following equation.

$$\xi = (P_p - P_c)/P_c, \tag{9}$$

where

P_p: load before dropping,

P_c: load after dropping.

When ξ is equal to 0.45, the fatigue crack almost stops, as shown in Fig.11(c). It can be seen that the numerical simulation gives valid results also in this case.

Figure 12 presents the numerical simulation results for fatigue crack propaga-

tion in a pre-existing residual stress field. Center notched specimens shown in Fig.12(a) were used in these experiments. Two types of residual stress distributions were considered in order to investigate the effect of the residual stress field on the fatigue crack growth behaviour. One specimen, further termed T specimen was heated along the center line (case A in Fig.12(a)) in order to generate a tensile residual stress near the notch tip. Another specimen, further termed C specimen (case B in Fig.12(a)) was simultaneously heated along both its edges in order to induce compressive residual stress at the notch tip. The resulting residual stress distributions measured by the stress relaxation method are shown in the lower part of Fig.12(a).

The fatigue crack propagation tests on these specimens and on a specimen without the pre-existing residual stress (named N specimen) were performed under the same applied constant amplitude loading with the maximum load of 27.46kN and the minimum load of 1.370 kN.

Figure 12(b) shows the estimated by the model and measured variations of the RPG load for each specimen. The RPG load for the T specimen is slightly lower than for the N specimen, while the RPG load for the C specimen is higher than for the N specimen. These results imply that the pre-existing tensile residual stresses prompt the crack to open and the pre-existing compressive stresses prompt the crack to close. In Fig.12(b), numerical calculations of P_{RPG} performed by applying measured residual stress distributions shown the solid lines in Fig.12(a).

Figure 12(c) shows the crack growth curves for each residual stress condition. The estimated curves are obtained based on the numerical results on the RPG load shown in Fig.12(b). It is evident in Fig.12(c) that the fatigue life can be

prolonged if a compressive residual stress field is generated near the crack initiation region. For specimen C, the estimated life is shorter than observed one. It is believed that this discrepancy is due to an insufficient accuracy of the residual stress measurements (the input to the model) rather than due to the model bad performance.

Figure 13 shows the effect of a spike overload on fatigue crack propagation [12].

The experimental results in Fig.13 confirm that the reterdation effect is proportional to the degree of spike loading. It can be anticipated that a sufficiently high overload will cause the crack arrest. The numerical simulation results are in a good agreement with the experimental data.

Figure 14 shows the observed and estimated from the model crack growth curves under a storm-simulating loading [15]. Two types of these type load histories are applied. Again a good agreement between the estimated and observed results is achieved.

Figure 15 [5] shows the relation between ΔK_{RPG} and the size of the overlapping region of the tensile plastic zone at P_{max} and the compressive plastic zone at P_{min} in a given loading cycle ($\tilde{\omega}$) for various loading conditions. From these results, the following relation is obtained.

$$\tilde{\omega} = \frac{\eta\pi}{8}\left(\frac{\Delta K_{RPG}}{2\lambda\sigma_Y}\right)^2, \tag{10}$$

where $\eta = 1.55$.

The shape of plastic region around a fatigue crack tip is affected by applied loading history. An example of the relation between loading history and plastic zone shape is shown in the center of Fig.16. Two types of the plastic region,

which are identified as case (I) and (II), can appear under cyclic loading. Case (I) appears in the ordinary loading condition, i.e. constant amplitude loading. Case (II) can appear just after enormous decrease of the loading amplitude as shown in Fig.16.

The difference of the plastic region shape should be considerd for evaluating the fatigue strength under variable loading, because both types of plastic region can appear randomly.

The fatigue crack does not propagate when $\tilde{\omega}$ is zero, because the plastic work is only consumed in the overlapping region of the plastic zones. It is understood that the threshold behaviour of a crack growth under arbitrary loading conditions is automatically represented by ΔK_{RPG}, without introducing ΔK_{th} or $(\Delta K_{eff})_{th}$. Moreover it is easily understood that $\tilde{\omega}$ increases as residual tensile deformed layer becomes small.

4 Concluding Remarks

A fatigue crack closure model to predict fatigue crack growth under an arbitrary unaxial stress field is proposed in this paper. The basic assumption behind this concept is that the fatigue crack growth in a fatigue cycle starts at an RPG load at which the tensile plastic zone ahead of the crack tip starts to develop.

Hence, the effective stress intensity factor range is redefined by replacing the crack opening load according to Elber with the RPG load. The novel crack driving force parameter based on the RPG load level is termed ΔK_{RPG}.

Unlike the traditional effective stress intensity factor range based on the crack opening level, the ΔK_{RPG} parameter can account for the threshold behaviour. Consequently, the crack growth rate versus ΔK_{RPG} data can be described using the Paris equation within the full range of crack growth, including the threshold region. The model has been shown to give accurate carck growth predictions under various constant and variable amplitude loading conditions and in the residual stress field.

Acknowledgements

This paper owes much to the thoughtful and helpful comments of Professor Malgorzata Skorupa, Faculty of Mechanical Engineering and Robotics, University of Mining and Metallurgy, Poland.

References

[1] Paris PC. and Erdogan F. A Critical Analysis of Crack Propagation Laws. Journal of Basic Engineering, Transactions of the ASME, Ser.D 1963:85:528–534.

[2] Dugdale DS. Yielding of Steel Sheets Containing Slits. Journal of Mechanics of Physics and Solids 1960:8:100–104.

[3] Elber W. The Significance of Fatigue Crack Closure. ASTM STP486 1971:230–242.

[4] Toyosada M., Yamaguchi K., Niwa T., Takenaka H., Kajimoto K. and Yajima H. Proposal of New Parameter for Fatigue Crack Propagation Rate based upon the Compliance Changing Phenomena and the Development of its measuring method. Journal of Society of Naval Architects of Japan 1991:169:245–255. (in

Japanese)

[5] Toyosada M., Niwa T., Gotoh K. and Sakai J. Physical meaning of ΔK_{RP} and assessment of fatigue crack propagation life for structures. Journal of Society of Naval Architects of Japan,1996, 180:539–547. (in Japanese)

[6] Toyosada M. and Niwa T. The Significance of RPG Load for Fatigue Crack Propagation and the development of a compliance measuring system. International Journal of Fracture, 1994, 67:217–230.

[7] Toyosada T., Gotoh K, Murakami K., Nakayama S. and Watanabe T. Physical meaning of the fictitious crack in Dugdale model. Transactions of the West-Japan Society of Naval Architects, 2003, 105:249-255. (in Japanese)

[8] Newman Jr. JC. A Crack-Closure Model for Predicting Fatigue Crack Growth under Aircraft Spectrum Loading. NASA Technical Memorandum 81941 1981.

[9] Machida S.,Toyosada, M. and Okamoto,T. Fatigue Crack Propagation under Various Types of Loading. Proceedings of the sixth International Conference of Fracture 1984:1743–1751.

[10] Newman Jr. JC.
FASTRAN-II: A FATIGUE CRACK GROWTH STRUCTURAL ANALYSIS PROGRAM. NASA Technical Memorandum 104156 1992.

[11] Toyosada M. and Niwa T. Simulation Model of Fatigue Crack Opening/Closing Phenomena for Predicting RPG Load under Arbitrary Stress Distribution Field. Proceedings of the fifth International Offshore and Polar Engineering Conference,1995, 169–176.

[12] Niwa T. and Toyosada M. A Study on Plastic Shrinkage Coefficient of Crack Opening/Closing model at a Crack Extension. Journal of Society of Naval Architects of Japan 2000:188:669–678. (in Japanese)

[13] Satoh K., Toyoda M. Itoh Y. Kawaguchi Y. Arimochi K. Suzuki M. and Tatara T. Fracture Transition Behaviors and Fracture Overall Strain of Low Carbon Steel Plate with Notch. Journal of Society of Naval Architects of Japan 1977:142:148–155. (in Japanese)

[14] Yada T., Sakai K., Iino N. and Sakano K. A Study on Elasto-plastic Behavior and Fracture Characteristics of Notched Plate Tensile Specimen. Journal of Society of Naval Architects of Japan 1973:145:425–435. (in Japanese)

[15] Tomita Y., Hashimoto K., Kariya Y., Pan Y. and Tadokoro S. The effect of time history of variable amplitude loading cycles on fatigue crack growth rate. Proceedings of the second International Offshore and Polar Engineering Conference (ISOPE'92), San Francisco, CA, USA, 1992,IV:282–287.

Figure 1 Plastic deformations and the working stress distribution along the crack line in one loading cycle during the fatigue crack propagation

Figure 2 Schematic view of the stress distribution near the crack tip just when the stress reaches yield stress under increasing load for cyclic loading and for monotonic loading

Figure 3 Crack propagation rates plotted against the effective stress intensity factor range based on the RPG load

Figure 4 Crack propagation rates plotted against the effective stress intensity factor range based on the crack opening load

Figure 5 Schematic change of the residual deformations and the working stress distribution along the crack line at threshold condition of crack growth

Figure 6 Illustration of the crack surface displacements for the fictitious crack from the Dugdale model and the approximation of the actual COD

Figure 7 Application of the superposition principle to computed COD in the plastic zone embedded in the previous plastic zone

Figure 8 Plastic shrinkage at the crack extension (for case C, no crack extension)

Figure 9 Explanaition of the meaning of parameter in Equation (7)

Figure 10 Effect of the stress ratio on crack propagation and comparison between the measured and simulated RPG load for mild steel

Figure 11 The change of RPG loads and crack growth after a step-down in maximum load decrease

Figure 12 Crack growth behaviour and the change of RPG load in pre-existing residual stress fields

Figure 13 Effect of spike overload on RPG load and fatigue crack propagation

Figure 14 Fatigue growth curves under two storm-simulation load histories

Figure 15 Relationship between the $\tilde{\omega}$ parameter and the effective stress in-

tensity factor range based on the RPG load

Figure 16 Illustration of the physical meaning of the $\tilde{\omega}$ parameter

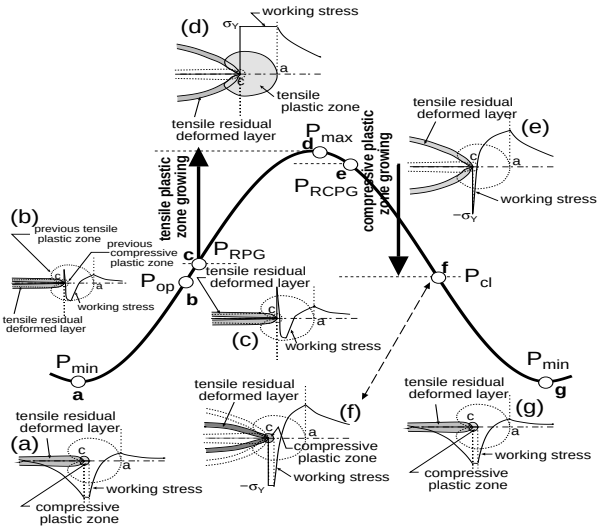

Figure 1

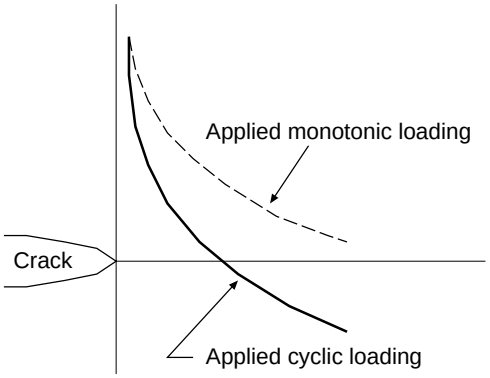

Figure 2

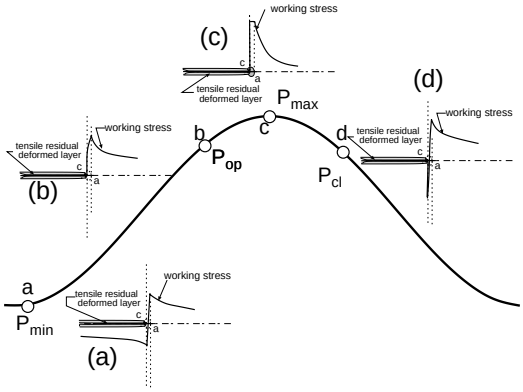

Figure 5

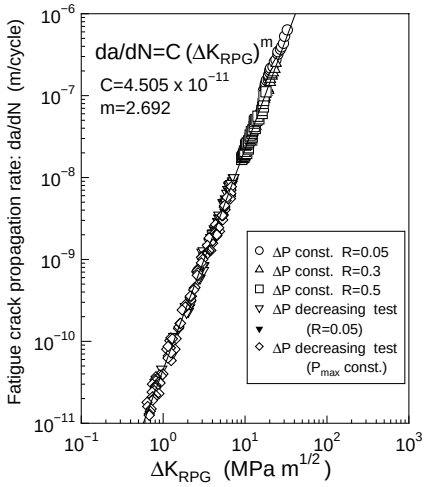

Figure 3

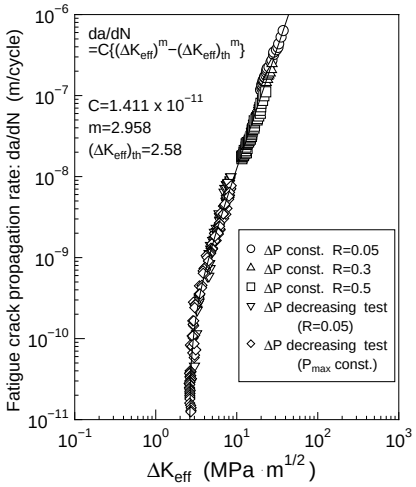

Figure 4

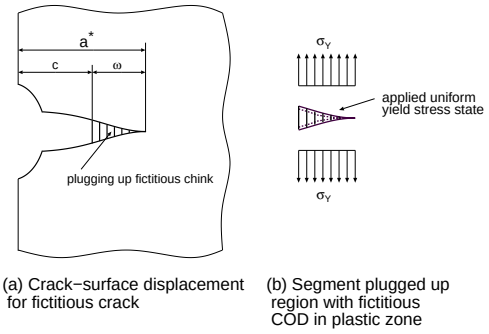

Figure 6

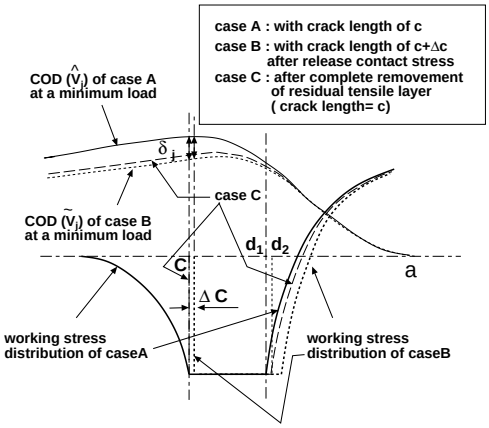

Figure 8

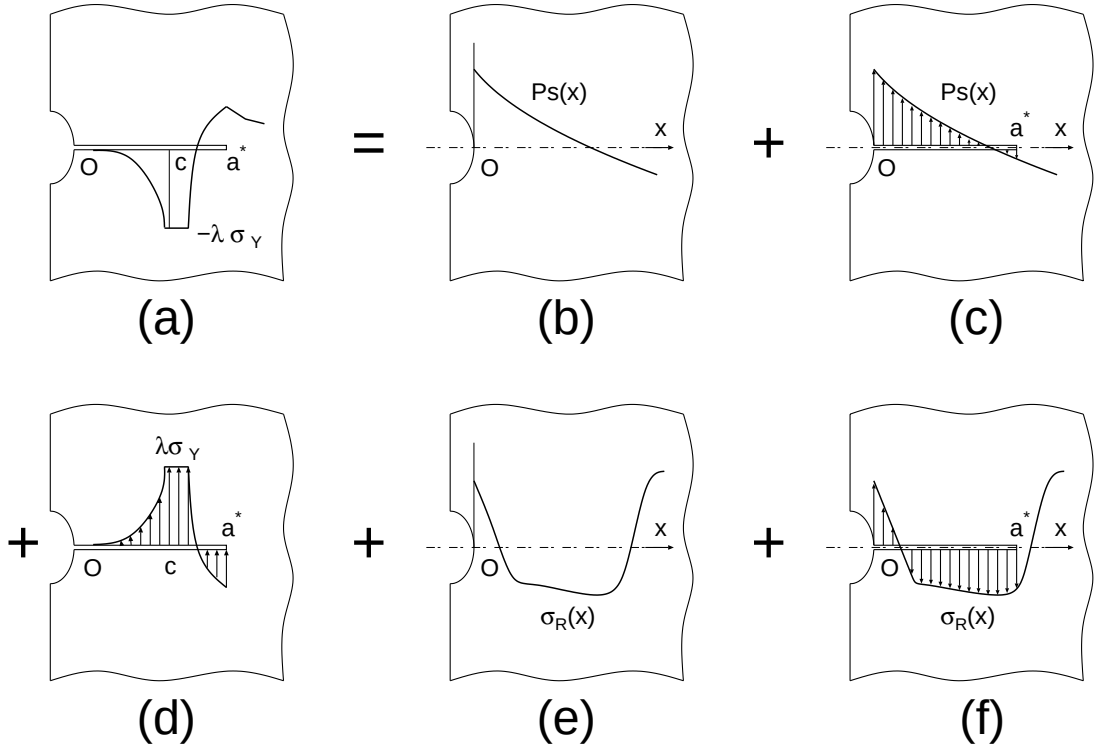

Figure 7

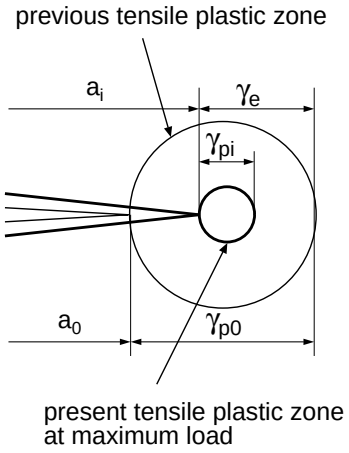

Figure 9

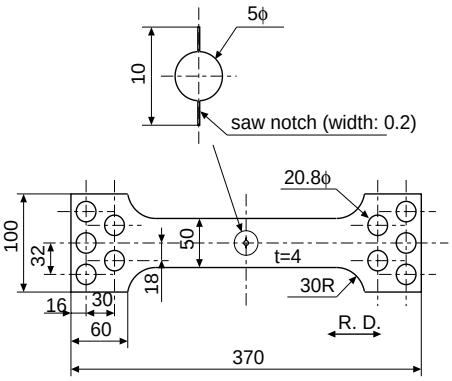

(a) Specimen configuration used

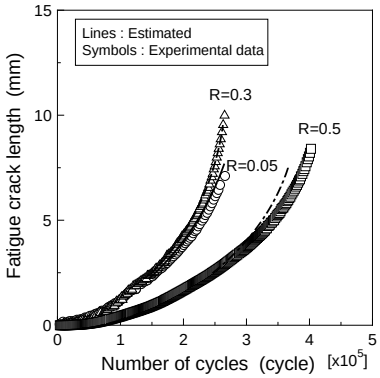

(b) Crack growth curves

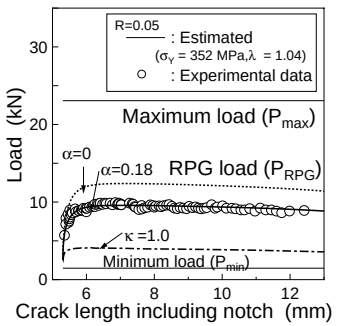

(c) RPG load (R=0.05)

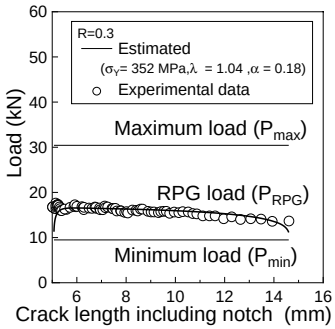

(d) RPG load (R=0.3)

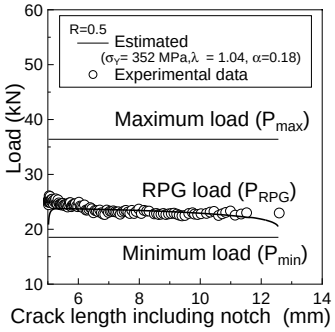

(e) RPG load (R=0.5)

Figure 10

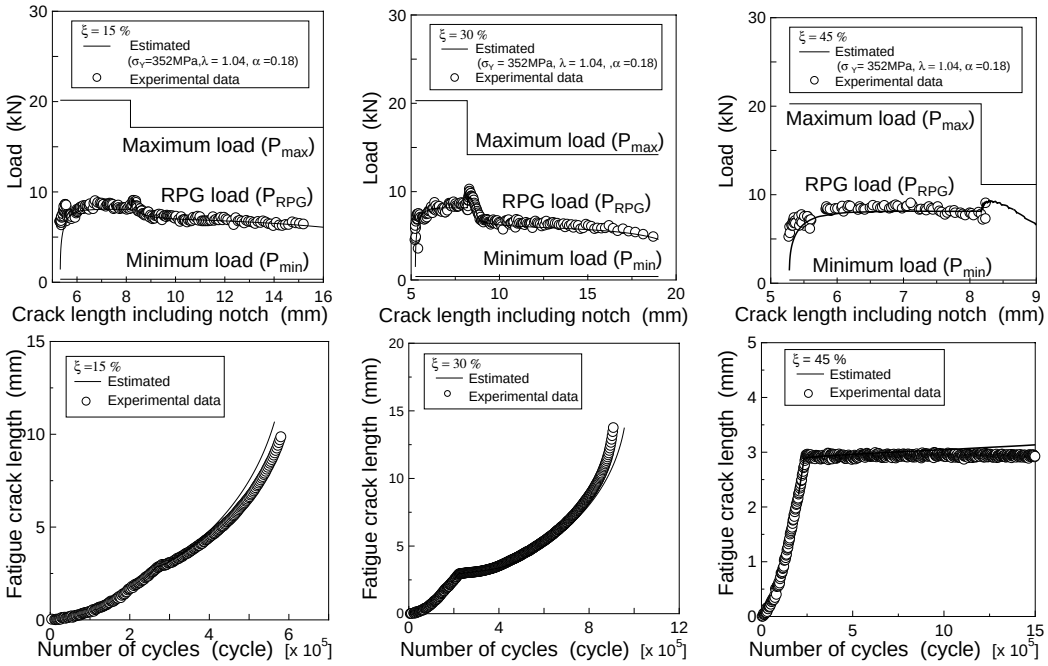

(a) $\xi = 15\%$ (b) $\xi = 30\%$ (c) $\xi = 45\%$

Figure 11

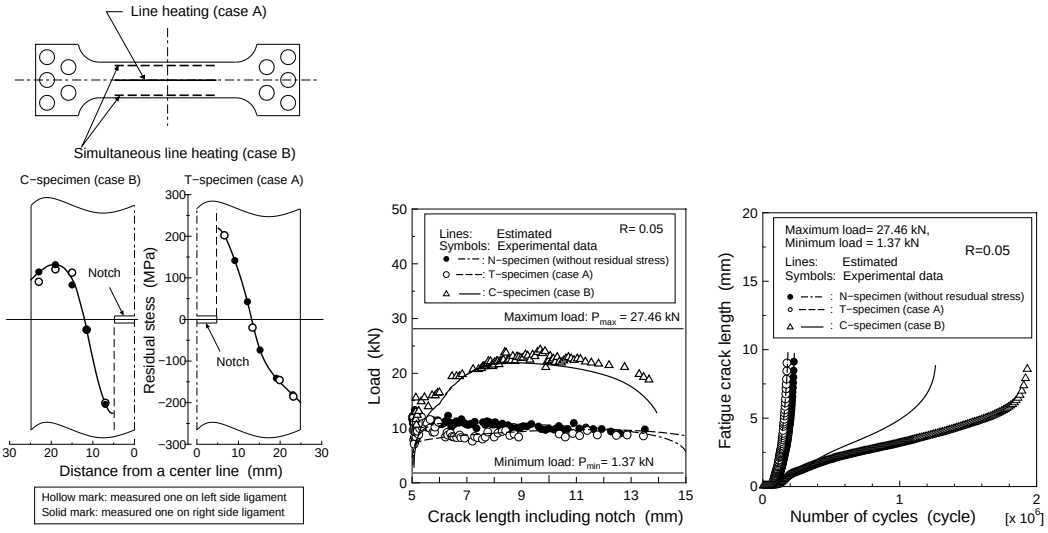

(a) Residual stress distribution (b) RPG load (c) Crack growth curves

Figure 12

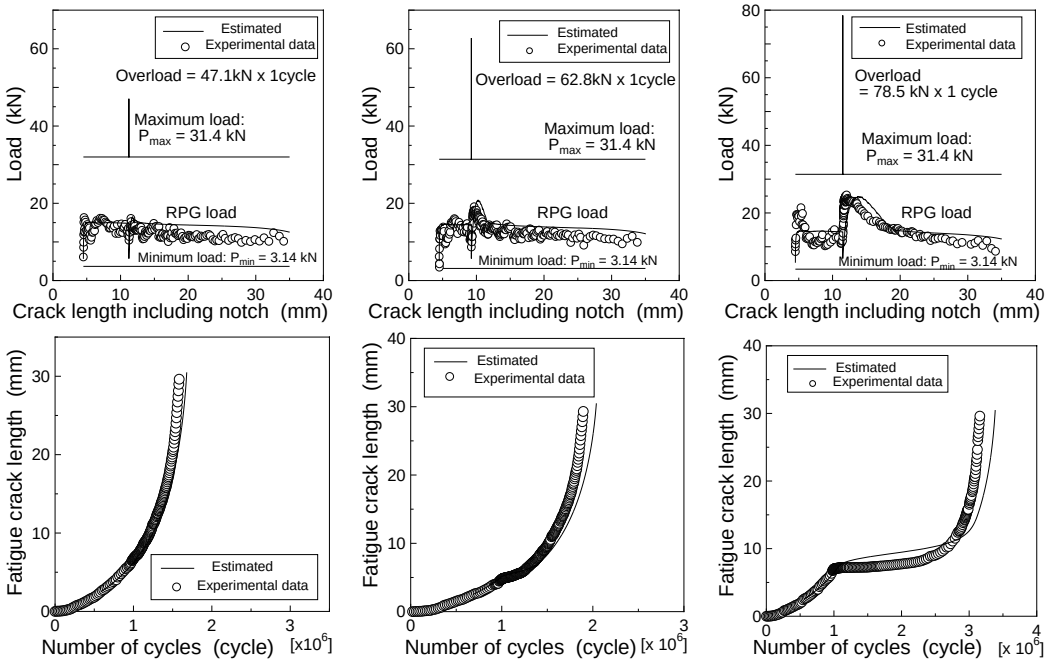

(a) spike load / maximum load = 1.5

(b) spike load / maximum load = 2.0

(c) spike load / maximum load = 2.5

Figure 13

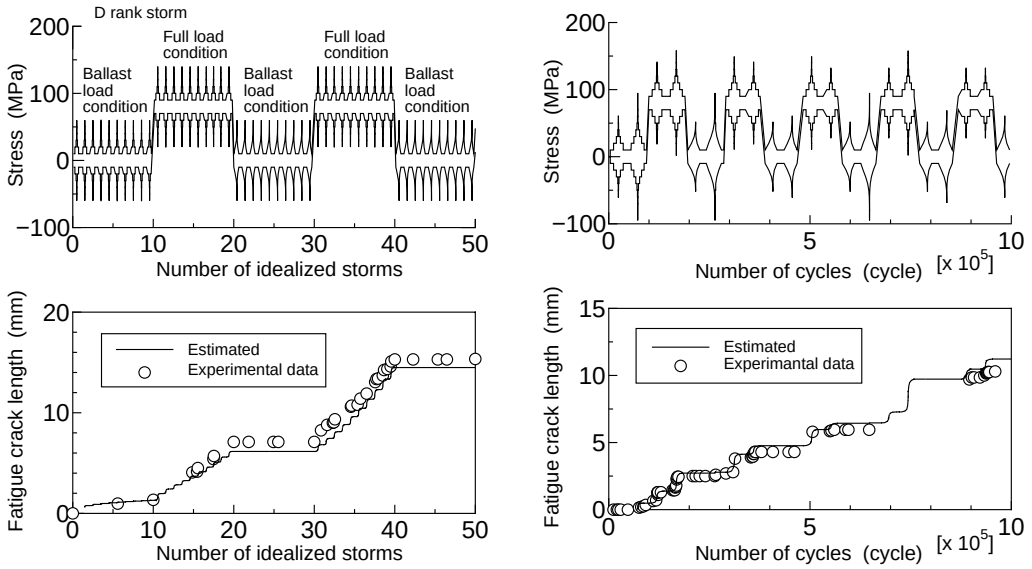

(a)

(b)

Figure 14

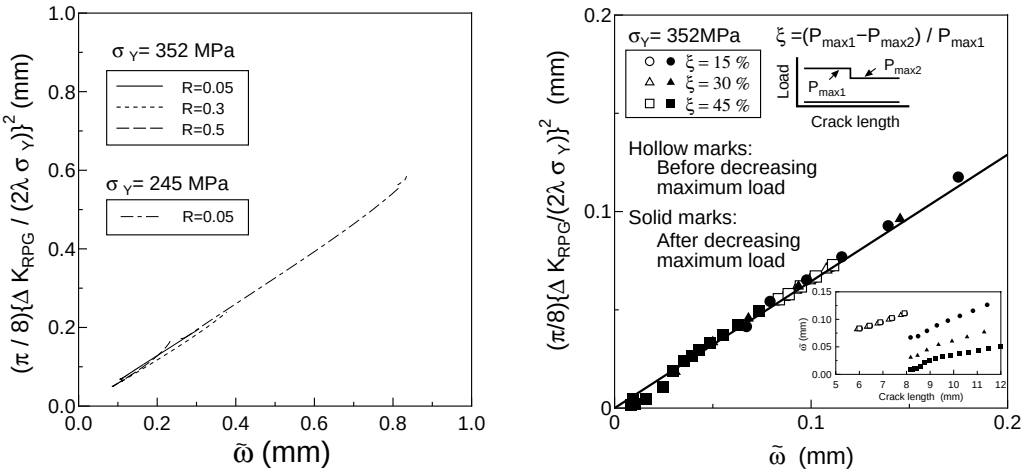

(a) Under constant amplitude loading (b) In case of decreasing maximum load

Figure 15

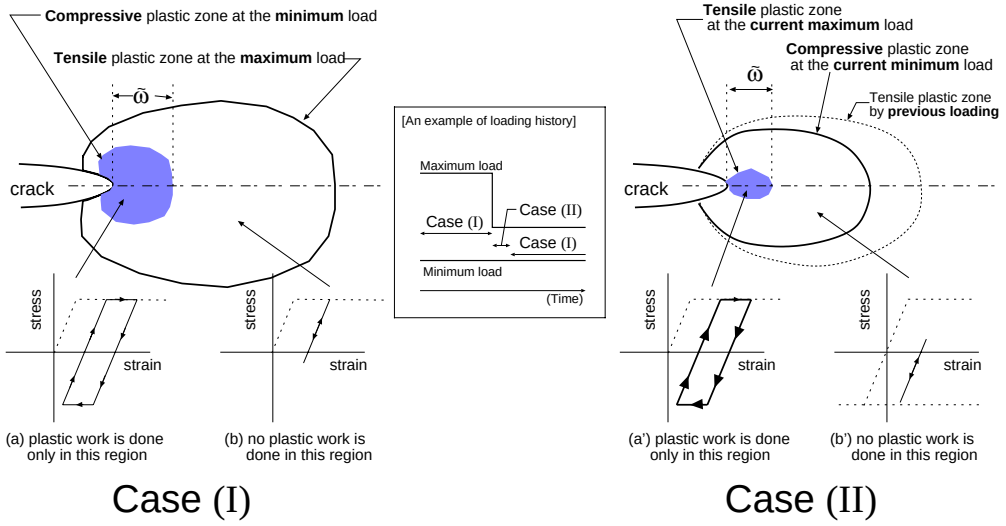

Figure 16